Chemistry SELECT

www.chemistryselect.org

A journal of ChemPubSoc Europe

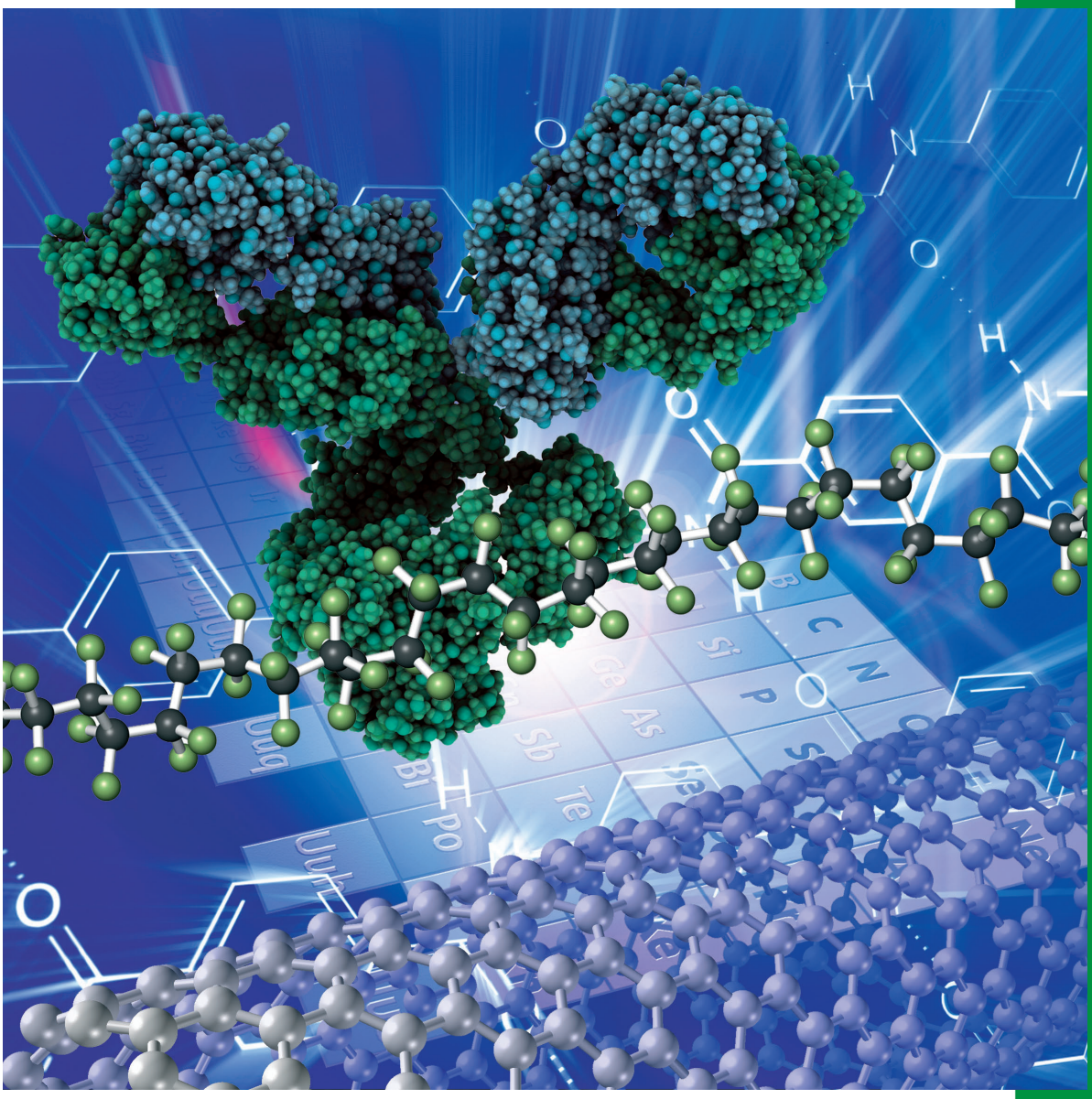

REPRINT

WILEY-VCH

Inorganic Chemistry

Ruthenium(II) Complexes of Isothiazole Ligands: Crystal Structure, HSA/DNA Interactions, Cytotoxic Activity and Molecular Docking Simulations

Maja B. Djukić,[a] Marija S. Jeremić,[a] Ignjat P. Filipović,[a] Olivera R. Klisurić,[b] Ratomir M. Jelić,[c] Suzana Popović,[d] Sanja Matić,[c] Valentina Onnis,[e] and Zoran D. Matović*[a]

Two new neutral ruthenium(II) complexes [Ru(η^6-*p*-cymene)Cl_2(**1**)] (**3**) and [Ru(η^6-*p*-cymene)Cl_2(**2**)] (**4**) (**1** = 5-(phenylamino)-3-pyrrolidin-1-ylisothiazole-4-carbonitrile; **2** = 3-morpholin-4-yl-5-(phenylamino)isothiazole-4-carbonitrile) have been synthesized and characterized using elemental analysis, IR, UV-Vis and NMR spectroscopy. The crystal structure was confirmed for complex **3** and both ligands. Examination of the interactions of ligands and complexes with CT-DNA (Calf Thymus DNA), as well as with HSA (Human Serum Albumin) revealed that ligands and complexes could interact with CT-DNA through intercalation and could bind strongly with HSA. Docking experiments toward DNA dodecamer indicate excellent accordance with experimental ΔG values. The cytotoxic activity of ligands and complexes was evaluated by MTT assay against HCT116 and HeLa tumoral cells. The complexes **3** and **4** showed good activity and selectivity on HCT116 cells. Neither of the tested compounds shows cytotoxic activity against a healthy MRC-5 cell line. Flow cytometry analysis showed the apoptotic death of the HCT116 cells with a cell cycle arrest in the S-phase.

1. Introduction

Some platinum drugs, such as Cisplatin, Oxaliplatin, and Carboplatin represent the best antitumor drugs of the last 45 years.[1–3] However, they show many side-effects including the risk of infection, dehydration, kidney toxicity, and many other abnormalities.[4] Also, many tumors show resistance to said drugs. That is why many research groups around the world have focused their research on syntheses of metal complexes that will show better antitumor activity with as few undesirable effects as possible. The experience of last decades indicates ruthenium(II)-*p*-cymene complexes with various ligands as possible alternatives.[5–8] Ruthenium(II) complexes are usually generally less toxic in comparison to Cisplatin so they have better potential as anticancer drugs.[9,10] Half-sandwich piano stool Ru^{II} complexes have attracted great interest in recent years for their antimetastatic and anticancer properties. However, two of them are examined in more detail: RAED–C ([Ru(η^6-*p*-cymene)(en)Cl]$^+$, where en = ethylenediamine) which is as cytotoxic as cisplatin targeting the DNA of chromatin[11] and RAPTA–C ([Ru(η^6-*p*-cymene)(PTA)]Cl_2], where PTA = 1,3,5-triaza-7-phosphaadamantane) which is anti-metastatic and anti-angiogenic agent able to form adducts with histone proteins.[12] Isothiazoles, on the other hand, represent an important class of aromatic organic ligands with nitrogen and sulfur in the adjacent position (Figure 1). These two electronegative heteroatoms allow very easy coordination of the five-membered aromatic heterocycle for different metal ions.[13] Isothiazole was

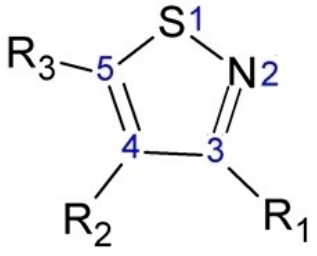

Figure 1. Structure of substituted isothiazole (R1, R2 and R3 = various atomic groups which may be part of the substituted isothiazole).

[a] *M. B. Djukić, Dr. M. S. Jeremić, I. P. Filipović, Prof. Z. D. Matović*
Department of Chemistry
Faculty of Science, University of Kragujevac
Radoja Domanovića 12, 34000 Kragujevac, Serbia
E-mail: zmatovic@kg.ac.rs
[b] *Prof. O. R. Klisurić*
Department of Physics
Faculty of Sciences, University of Novi Sad
Trg Dositeja Obradovića 4, 21000 Novi Sad, Serbia
[c] *Prof. R. M. Jelić, S. Matić*
Department of Pharmacy
Faculty of Medical Sciences, University of Kragujevac
Svetozara Markovića 69, 34000 Kragujevac, Serbia
[d] *Dr. S. Popović*
Centre for Molecular Medicine and Stem Cell Research
Faculty of Medical Sciences, University of Kragujevac
Svetozara Markovića 69, 34000 Kragujevac, Serbia
[e] *Prof. V. Onnis*
Department of Life and Environmental Sciences
Unit of Pharmaceutical, Pharmacological and Nutraceutical Sciences, University of Cagliari
University Campus, S.P. n° 8, Km 0.700, I-09042 Monserrato (CA), Italy

Supporting information for this article is available on the WWW under https://doi.org/10.1002/slct.202002670

first synthesized in 1956[14] and since then its chemical and physical properties have been extensively studied, as well as its derivatives.[15,16] They showed a wide range of useful properties which led researchers to study the synthesis and chemical transformations of its derivatives. Isothiazole derivatives are widely used in medicine mainly as antiviral, antimicrobial, and fungicidal agents,[15c,17–19] while data on antitumor activity is very scarce.[20–23] Among isothiazoles, aminoisothiazole derivatives have been reported for their biological activity. Different molecules bearing the aminoisothiazole moiety demonstrate activity against cancer cell proliferation as antimitotic agents,[24] cyclin-dependent kinases[25] and ATP-competitive inhibitors of kinases.[26]

Herein, crystal structures of the two synthesized isothiazole ligands **1** and **2** have been described. Also, two new structurally similar piano-stool ruthenium(II)-*p*-cymene complexes, [Ru(η^6-*p*-cymene)Cl_2(**1**)] (**3**) (**1** = 5-(phenylamino)-3-pyrrolidin-1-ylisothiazole-4-carbonitrile) and [Ru(η^6-*p*-cymene)Cl_2(**2**)] (**4**) (**2** = 3-morpholin-4-yl-5-(phenylamino)isothiazole-4-carbonitrile) have been synthesized, characterized using spectroscopic methods and systematically investigated for their biological reactivity. The crystal structure was confirmed only for complex **3**, as well as for both ligands. Additionally, the results of in vitro cytotoxicity for the two ligands and the two complexes against two cancer cell lines and one non-cancer cell are reported. Also, we examined the in vitro interaction of the ligands and their complexes with calf thymus DNA (CT-DNA), as well as the in vitro affinity of the ligands and their complexes for human serum albumin (HSA) by UV-Vis spectroscopy and fluorescence emission spectroscopy. Furthermore, docking simulations toward DNA dodecamer have been done to establish binding energies of the Ligand-DNA system.

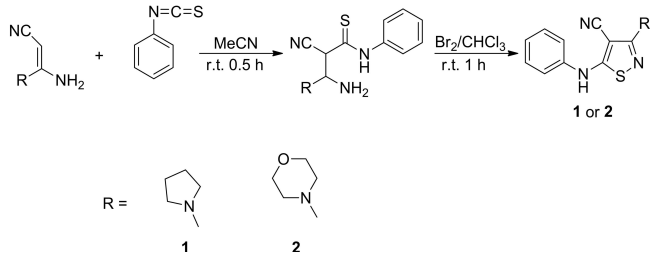

Scheme 1. Synthetic route for ligands **1** and **2**.

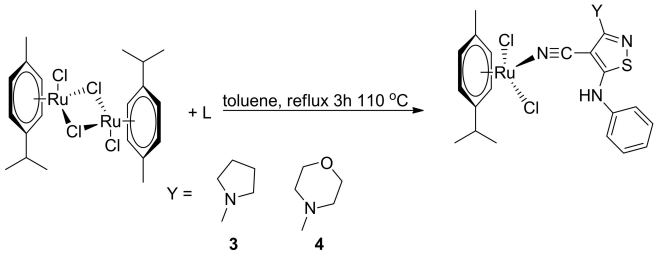

Scheme 2. Synthetic route for complexes **3** and **4**.

2. Results and Discussion

2.1. Synthesis and spectral characterization

The 3,5-diaminoisothiazole derivatives **1** and **2** were prepared in excellent yields by our previously reported protocol (Scheme 1).[16b]

These ligands **1** and **2** were used for synthesis with the [Ru-(η^6-*p*-cymene)Cl_2]$_2$ in the presence of toluene under reflux (Scheme 2). The corresponding ruthenium(II) complexes were obtained as orange microcrystalline solid of [Ru(η^6-*p*-cymene)Cl_2(**1**)] (**3**) suitable for X-ray analysis and as orange powder of [Ru(η^6-*p*-cymene)Cl_2(**2**)] (**4**). The complexes were also characterized by elemental analysis, IR, UV-Vis, and NMR spectroscopy (Figure 2 and Figures S1-S6 in the Supporting Information). The IR spectra show that the coordination of the ligands for ruthenium(II)-ion was achieved via the -C≡N group. This band is located at a higher frequency relative to the same band in the spectra of the uncoordinated ligands (Figure 2). UV-Vis spectra for both complexes were recorder from 200–800 nm in methanol and show a single strong peak at 429 nm (complex **3**) and 431 nm (complex **4**). These peaks could be assigned to the metal to ligand (dπ-π*) charge transfer (MLCT) transition from the filled 4d orbital to the empty π* orbital, similar to the MLCT observed in other reported Ru(II)-arene complexes.[27] The NMR spectra were recorded in $CDCl_3$ to confirm the bonding of the ligand to the ruthenium(II) ion. In the ^{1}H NMR spectra of both complexes, a multiplet appeared at the region 7.08–7.40 ppm (complex **3**) and 7.11–7.42 ppm (complex **4**) has been assigned to a phenyl group. The complex **3** shows two multiplets originating from protons belonging to pyrrolidine (δ = 1.97–2.04 ppm and δ = 3.62–3.69 ppm), while complex **4** show two triplets at 3.56 ppm and 3.82 ppm which is derived from morpholine protons. All the other signals belong to ruthenium-*p*-cymene. ^{13}C NMR spectra show the corresponding number of signals relative to the structure of the compound.

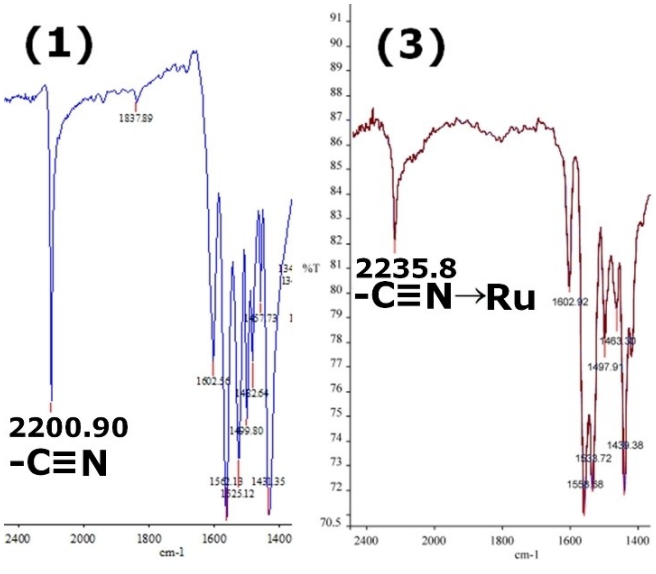

Figure 2. IR spectra of ligand **1** (left) and complex **3** (right).

2.2. Crystal structures

A perspective view of the molecular structure of complex **3** with an adopted atom-numbering scheme is shown in Figure 3. Selected bond lengths, bond angles, and torsion angles are listed in Table 1.

Complex **3** crystallizes in the triclinic crystal system and $P^{-}1$ space group where each asymmetric unit consists of the one neutral form of Ru-*p*-cymene-complex. In the crystal structure of the complex **3** the Ru^{II} ion is coordinated by two Cl^{-} ions and nitrogen donor atom of ligand **1** with the Ru1-N1 bond distance of 2.059 (2) Å and Ru1-$Ar_{centroid}$ bond distance (π bond) with the value of 1.664 Å. The crystal structure of the complex **3** is stabilized by intramolecular hydrogen bond involving NH group and $(Cl2)^{-}$ ion (Table S1 in the Supporting Information).

The molecular structures of ligands **1** and **2** are presented in Figure 4 while the selected bond lengths and bond angles are presented in Table 2. Both ligands crystallize in the monoclinic crystal system where **1** in $P2_1/n$ and **2** in $P2_1/c$ space group. Validation of the conformation of ligand structures through the values of dihedral angles (Table 2) is showing that the isothiazole-4-carbonitrile part in ligands **1** and **2** can be considered almost perfectly planar. On the other hand, the angles between ring planes C2-C3-S1-N2-N4 and C9-C10-C11-C12-C13-C14 in **1** (7.22°) and **2** (27.08°) are showing that the molecular structure of ligand **2** deviates from planarity decidedly more compared to the structure of ligand **1**. Pyrrolidine and morpholine part in **1** and **2**, respectively, gives rise to conformational differences since five-membered pyrrolidine in **1** has twist conformation with puckering parameters $q_2 = 0.330(2)$ Å, $\phi_2 = -130.7(4)°$ while the morpholine in **2** is adopting the chair conformation where the puckering parameters are: QT = 0.5598(18) Å, $\theta_2 = 2.12(17)°$. The crystal packing of ligand **1** consists of doubly N–H···N hydrogen-bonded dimmers forming layers along *b* axis (Figure 5, Table S1 in the Supporting Information) while the molecules of **2** in the crystal structure are connected in a head-to-tail manner by intermolecular N–H···O hydrogen bonds (Figure 5, Table S1 in the Supporting Information).

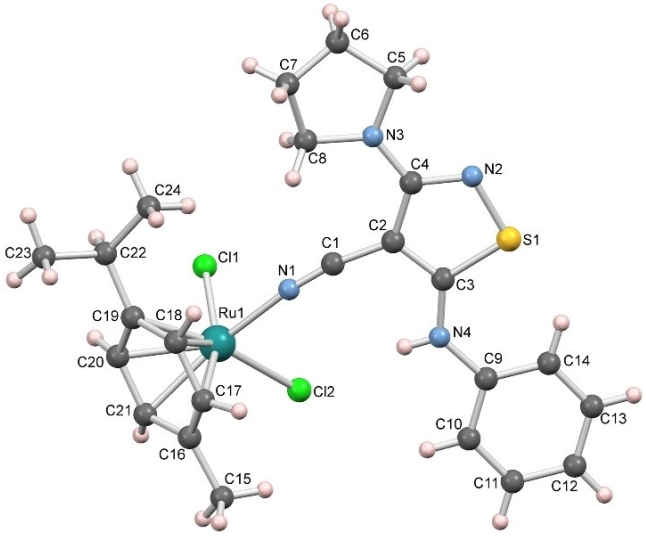

Figure 3. MERCURY[28] drawing of the molecular structure of the complex **3**.

Table 1. Selected geometric parameters for complex **3**.

Bond length [Å]			
Ru1-N1	2.059 (2)	S1-N1	1.655 (3)
Ru1-C18	2.150 (3)	S1-C3	1.722 (3)
Ru1-C20	2.159 (3)	N1-C1	1.134 (3)
Ru1-C19	2.176 (3)	N4-C3	1.357 (4)
Ru1-C21	2.190 (3)	N4-C9	1.392 (4)
Ru1-C17	2.195 (3)	N2-C4	1.325 (4)
Ru1-C16	2.211 (3)	N3-C4	1.341 (5)
Ru1-Cl1	2.409 (8)	N3-C8	1.448 (5)
Ru1-Cl2	2.428 (8)	N3-C5	1.462 (4)
Bond angles [°]			
Cl1-Ru1-Cl2	88.57 (3)	C3-C2-C1	118.26 (3)
N1-Ru1-Cl1	86.00 (7)	C3-C2-C4	112.42 (3)
N1-Ru1-Cl2	82.60 (7)	C1-C2-C4	129.42 (3)
N1-Ru1-C18	89.78 (1)	N2-C4-N3	120.64 (3)
N1-Ru1-C20	145.75 (1)	N2-C4-C2	114.08 (3)
N1-Ru1-C21	165.08 (1)	N3-C4-C2	125.27 (3)
C19-Ru1-Cl1	94.06 (8)	N4-C3-C2	125.27 (3)
C21-Ru1-Cl1	108.75 (8)	N4-C3-S1	127.33 (3)
C18-Ru1-Cl2	143.89 (9)	C2-C3-S1	107.30 (2)
Torsion angles [°]			
Ru1-C21-C16-C17	54.5 (2)	N1-C1-C2-C3	-1.0 (2)
Ru1-C21-C16-C15	−123.6 (3)	N1-C1-C2-C4	178.4 (2)
Ru1-C19-C18-C17	−54.9 (2)	S1-N2-C4-N3	-177.9 (3)
Ru1-C18-C17-C16	−52.5 (2)	S1-N2-C4-C2	0.6 (4)
Ru1-C19-C22-C24	−58.7 (4)	C8-N3-C4-N2	-169.8 (3)
Ru1-C19-C22-C23	176.8 (3)	C5-N3-C4-N2	-0.6 (6)
Ru1-C16-C17-C18	51.3 (2)	C8-N3-C4-C2	11.8 (6)
C5-N3-C4-C2	−178.9 (4)		

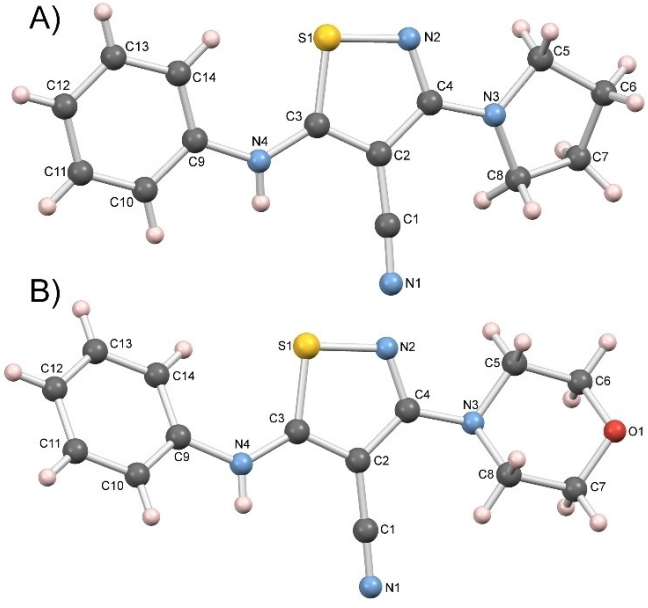

Figure 4. MERCURY[28] drawings of the molecular structure of ligands: *A*) **1** and *B*) **2** with labeled non-H atoms.

Table 2. Selected geometric parameters for ligands **1** and **2**.

Bond length [Å]		
	1	**2**
S1-N2	1.658 (2)	1.656 (2)
S1-C3	1.720 (2)	1.719 (2)
N4-C3	1.357 (3)	1.346 (2)
N4-C9	1.393 (3)	1.410 (2)
N3-C4	1.345 (3)	1.383 (2)
N3-C8	1.456 (3)	1.460 (2)
N3-C5	1.461 (3)	1.467 (2)
N2-C4	1.324 (2)	1.313 (2)
N1-C1	1.144 (2)	1.140 (2)
O1-C7	/	1.413 (2)
O1-C6	/	1.429 (2)
Bond angles [°]		
N2-S1-C3	95.70 (9)	95.08 (8)
C3-N4-C9	131.08 (2)	128.44 (2)
C4-N3-C8	125.23 (2)	117.32 (1)
C4-N3-C5	120.30 (2)	114.86 (2)
C8-N3-C5	111.77 (2)	110.84 (1)
C4-N2-S1	110.28 (1)	110.65 (1)
C3-C2-C1	120.80 (2)	122.04 (2)
C3-C2-C4	111.62 (2)	110.94 (2)
C1-C2-C4	127.55 (2)	126.89 (2)
N2-C4-N3	120.20 (2)	119.72 (2)
C7-O1-C6	/	109.18 (2)
O1-C6-C5	/	111.92 (2)
Torsion angles [°]		
C3-S1-N2-C4	0.8 (2)	0.6 (2)
S1-N2-C4-N3	178.3 (2)	178.6 (1)
S1-N2-C4-C2	−1.8 (2)	0.0 (2)
C8-N3-C4-N2	−162.5 (2)	135.8 (2)
C5-N3-C4-N2	−2.7 (3)	3.0 (2)
C8-N3-C4-C2	17.7 (3)	−45.7 (3)
C5-N3-C4-C2	177.4 (2)	−178.6 (2)
C3-C2-C4-N2	2.2 (3)	−0.7 (2)
C1-C2-C4-N2	−175.8 (2)	175.3 (2)
C7-O1-C6-C5	/	59.1 (2)
N3-C5-C6-O1	/	−56.8 (2)

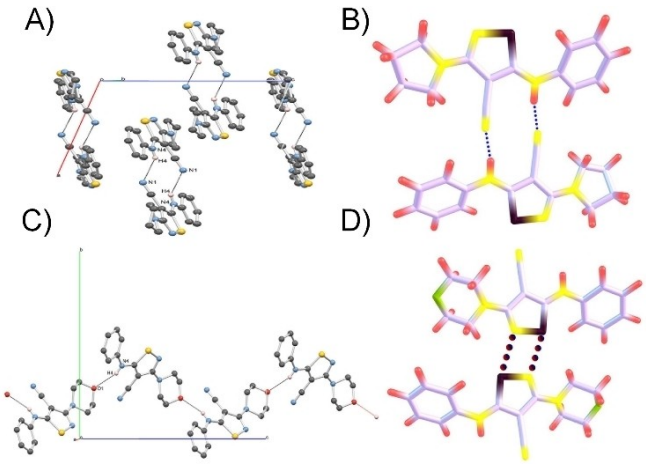

Figure 5. The crystal packing of ligand **1** viewed along the *b*-axis. Hydrogen bonds are shown as black dashed lines. The molecules of **1** are connected in dimmers by N4–H4···N1 [$-x+2$, $-y+1$, $-z+1$] hydrogen bond (*A*). Dimmer associated with close contacts of N–H atoms originated from different molecules (*B*). The crystal packing of ligand **2** viewed along the a-axis. Hydrogen bonds are shown as black dashed lines. The molecules of **2** are connected in a head-to-tail manner by N4–H4···O1 [1–*x*,1/2+*y*, 3/2-*z*] hydrogen bond (*C*). Dimmer associated with close contacts of N–S atoms originated from different molecules (*D*).

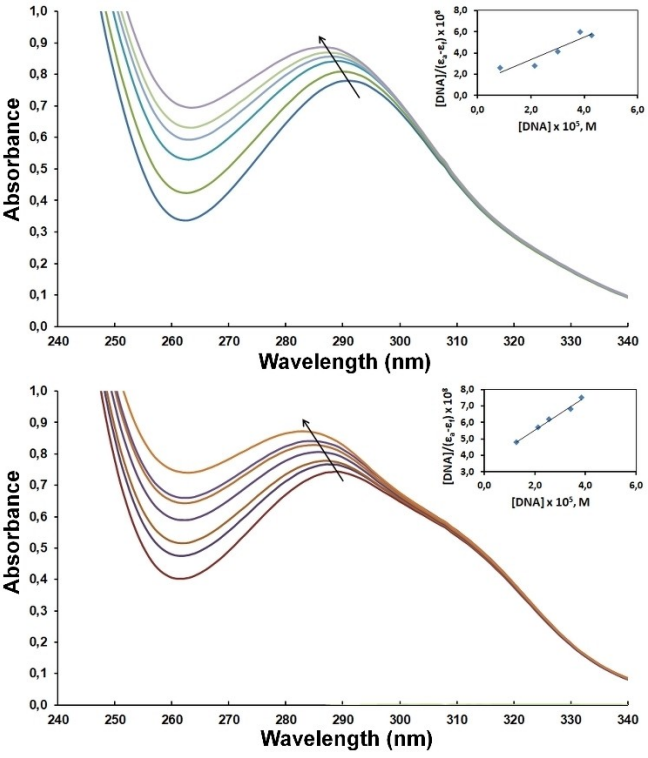

Figure 6. Electronic absorption spectra of complexes **3** (up) and **4** (down) in Tris-HCl buffer upon the addition of CT-DNA. [Complex] = 40 μM, [DNA] = 0–40.3 μM. The arrow shows the absorption intensities increase upon increasing DNA concentration. Inset: plot of [DNA]/(ε_a–ε_f) vs. [DNA].

2.3. DNA binding experiments

The determination of the interactions between small molecules and DNA is important in pharmacology when evaluating the potential of new antitumor complexes,[29] and therefore interactions between DNA and the synthesized complexes should be investigated. The mode and strength for the binding of the synthesized ligands and their complexes with ruthenium(II) to CT-DNA were studied with UV-Vis and fluorescence spectroscopic methods.

2.3.1. Electronic absorption spectra

UV-Vis absorption measurement is a very simple but effective method that is used to investigate mode of interaction between metal complexes and DNA.[30] Interaction of metal complexes with base pairs of the DNA is usually followed by hypo- or hyperchromic shift with a small red/blue shift.[31] The extent of the hyperchromism in the absorption band is generally consistent with the strength of intercalative binding/interaction.[32] The absorption spectra of complexes in the absence and presence of CT-DNA are given in Figure 6 and Figures S7 and S8 in the Supporting Information. The absorption intensities increase upon increasing DNA concentration in

the investigated complexes, the absorption band of complexes at 290 nm exhibited hyperchromism with blue shifts of 3 to 5 nm. These results indicate that the observed spectral changes may be explained by the intercalative binding of the complex to DNA.[33]

In order to further compare the binding strength of the ruthenium(II) complexes, their intrinsic binding constants (K_b) were determined from the following Equation (1):[34]

$$\frac{[DNA]}{\varepsilon_a - \varepsilon_f} = \frac{[DNA]}{\varepsilon_b - \varepsilon_f} + \frac{1}{K_b(\varepsilon_b - \varepsilon_f)} \quad (1)$$

where [DNA] is the concentration of DNA in base pairs, the apparent absorption coefficients ε_a, ε_f and ε_b correspond to A_{obsd}/[complex], the extinction coefficient for the free complex and the extinction coefficient for the complex in the fully bound form, respectively. The intrinsic binding constant (K_b) values were 8.28×10^4 M^{-1} (R = 0.935) and 4.54×10^4 M^{-1} (R = 0.993), for complexes 3 and 4, and 3.18×10^4 M^{-1} (R = 0.919) and 3.70×10^4 M^{-1} (R = 0.987), for ligands 1 and 2 respectively (Table 3). From the results obtained, it has been found that complex 3 binds more strongly with CT-DNA compared to the complex 4.

2.3.2 Ethidium bromide (EB) displacement studies

Absorption results show that the complexes bind to DNA. In order to examine the ability of the ligands and their complexes to displace EB from the EB-DNA complex, competitive EB binding studies were carried out with fluorescence measurements. The compounds competing with EB to intercalate with DNA will induce the displacement of the bound EB, decreasing the fluorescence intensity. EB is a typical indicator of intercalation that forms soluble complexes with nucleic acids and emits intense fluorescence in the presence of CT DNA.[35] The emission spectra of EB bound to CT-DNA in the absence and presence of compounds were recorded and are shown in Figure 7 and Figure S9 in the Supporting Information. Fluorescence intensity of EB bound to DNA at 613 nm shows decreasing trend with the increasing concentration of the compound.

The observed decrease in the fluorescence intensity indicates that the EB molecules are displaced from their DNA binding sites and were replaced by the compounds tested. The quenching parameter can be analyzed according to the Stern-Volmer equation:[36]

$$\frac{F_0}{F} = 1 + k_q\tau_0[Q] = 1 + K_D[Q] = 1 + K_{SV}[Q] \quad (2)$$

of the diagram F_0/F versus [Q]. The K_{SV} values were obtained from the slope in the plot of F_0/F versus [Q] (see inset in Figure 7 and Figure S9 in the Supporting Information). The obtained K_{SV} constants in presence of compounds were 3.57×10^4 M^{-1} (R = 0.949) for complex 3 and 3.78×10^4 M^{-1} (R = 0.912) for complex 4 and 3.02×10^4 M^{-1} (R = 0.997) for ligand 1 and 3.41×10^4 M^{-1} (R = 0.982) for ligand 2. The ligand 1 and corresponding complex 3 exhibit a lower K_{SV} value than the ligand 2 and corresponding complex 4 and have a lower ability to displace EB from CT DNA-EB complex. The values of K_q (3.57×10^{12} M^{-1} for 3 and 3.78×10^{12} M^{-1} for 4 and 3.02×10^4 M^{-1} for 1 and 3.41×10^4 M^{-1} for 2) were greater than 10^{10} M^{-1} s^{-1}, indicating that the quenching mechanism, as a result of the formation of the CT DNA-EB-complex, is a static quenching process.

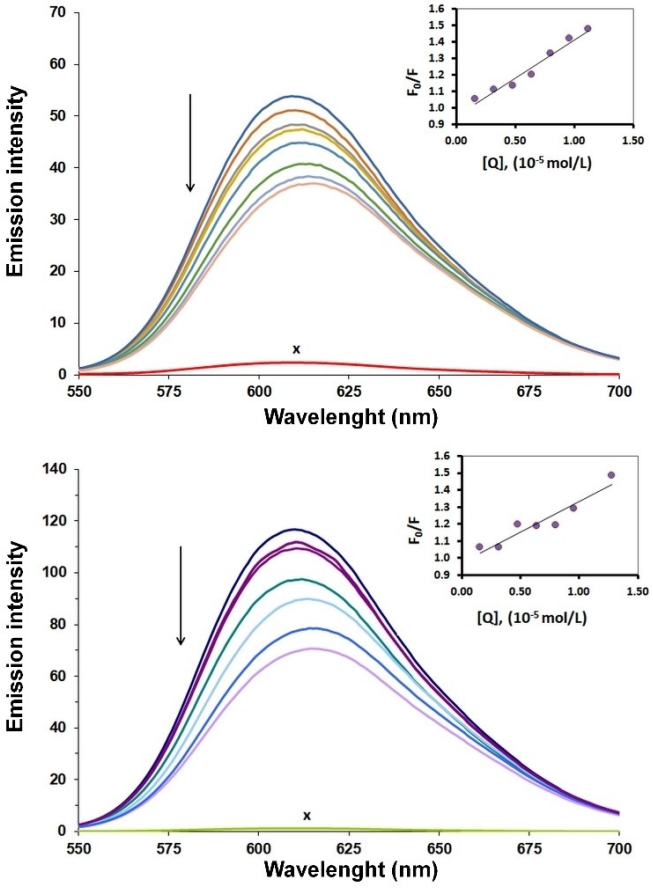

Figure 7. Fluorescence emission spectra (λ_{ex} = 520 nm) of ethidium bromide bound to DNA: ligand **1** (up) and complex **3** (down). [DNA] = 22 μM, [EB] = 20 μM, and [compound] = 0–13 μM. Arrow shows the emission intensity changes upon increasing complex concentration. x represents 13 μM compound only. Inset: plot of F_0/F vs. [compound].

Table 3. The DNA binding constants (K_b), calculated from UV spectra and the Stern-Volmer constants (K_{sv}), and Quenching constant (K_q) calculated from fluorometric spectra.

Compd.	In the absence of EB		In the presence of EB		
	K_b[a]	R[b]	K_{SV}[a]	K_q[c]	R[a]
1	3.18×10^4	0.919	3.02×10^4	3.02×10^{12}	0.997
2	3.70×10^4	0.987	3.41×10^4	3.41×10^{12}	0.982
3	8.28×10^4	0.935	3.57×10^4	3.57×10^{12}	0.949
4	4.54×10^4	0.993	3.78×10^4	3.78×10^{12}	0.912

[a] M^{-1}. [b] R is the correlation coefficient. [c] M^{-1}s^{-1}.

2.4. Interaction of the ligands and complexes with albumin

It has been proved that the most important role of the serum albumins is the transportation of metal ions and metal complexes as well as other biologically active compounds in the blood. The investigation of binding interactions between the potentially active compounds and HSA can be important in exploring their potential biological activity and application. In order to investigate the structural changes in HSA caused by the addition of ligand or complex and determine the quenching constants (k_q), the binding constant (K) and the number of binding sites (n) for the complex formed between ligand or complex and HSA, absorption and fluorescence spectra were measured.

HSA solutions exhibit a strong fluorescence emission with a peak at about 350 nm, due to the tryptophan residues, when excited at 295 nm.[37] The fluorescence spectra of HSA with different concentrations of ligands 1 and 2, and complexes 3 and 4 were recorded and are shown representatively for complex 3 in Figure 8 (others are shown in Figures S10–S12 in the Supporting Information). As shown in Figures 8 and S10–S12, adding complex to the HSA solution, the fluorescence intensity of HSA decreased gradually with an increase in complex concentration. This result suggests that complex can interact with HSA and quench its intrinsic fluorescence. Furthermore, fluorescence quenching data were analyzed with the Stern-Volmer equation (Equation (2)), similarly as described above for DNA binding experiments. From the plot of F_0/F versus [Q] the K_{SV} and the quenching constants (k_q) can be calculated (see inset in Figure 8 and Figures S10-S12 in the Supporting Information), where the fluorescence lifetime of tryptophan in HSA was taken as $\tau_0 = 10^{-8}$ s.

If it is assumed that the binding of compounds with HSA occurs at equilibrium, the equilibrium binding constant (K) and the binding stoichiometry (n) of HSA–compounds system can be estimated by the following Equation (3)[36] using the fluorescence intensity data:

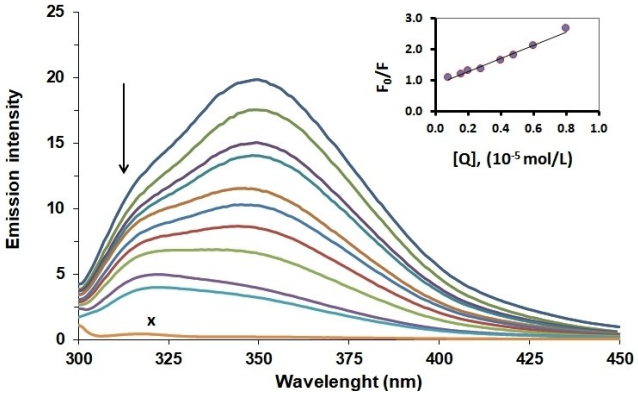

Figure 8. Fluorescence emission spectra of HSA in the presence of various concentrations of complex **3** ($T = 298$ K, pH 7.4). [HSA] = 2.0 μM. [complex] = 0-16 μM. Curve x shows the emission spectrum of complex **3** only. The arrow shows the intensity change upon the increase of the complex concentration. Inset: plot of F_0/F vs. [complex].

$$\log\frac{F_0 - F}{F} = \log K + n\log[Q] \quad (3)$$

The values of K and n were obtained from the intercept and slope of the plots of log $(F_0 - F)/F$ versus log [Q] (Figure 9 and Figure S13 in the Supporting Information).

Fluorescence intensities were corrected for the absorption of exciting light and reabsorption of the emitted light to decrease the inner filter effect using the Equation (4):[36]

$$F_{cor} = F_{obs} \times 10^{\frac{A_{ex}+A_{em}}{2}} \quad (4)$$

where F_{cor} and F_{obs} represent the corrected and observed fluorescence intensities, and A_{ex} and A_{em} are the absorbance of protein and ligand at the excitation and emission wavelengths, respectively.

The calculated K_{SV}, k_q, K, and n values are given in Table 4. As seen in Table 4, the quenching constants ($> 10^{12}$ $M^{-1}s^{-1}$) are higher than diverse kinds of quenchers for biopolymers fluorescence (10^{10} $M^{-1}s^{-1}$), suggesting that the interaction of the ligands and complexes with the albumins takes place via a static quenching mechanism, which indicates the formation of a new conjugate between each complex and HSA.[38]

The calculated value of n is around one for all the compounds, indicating the existence of just a single binding site in HSA for all the compounds. From the values of K_{SV} and K, it is inferred that complex 3 interacts with HSA more strongly than the rest of the compounds. The binding constant (K) of complexes 3 and 4 (see Table 4) showed that there is a good

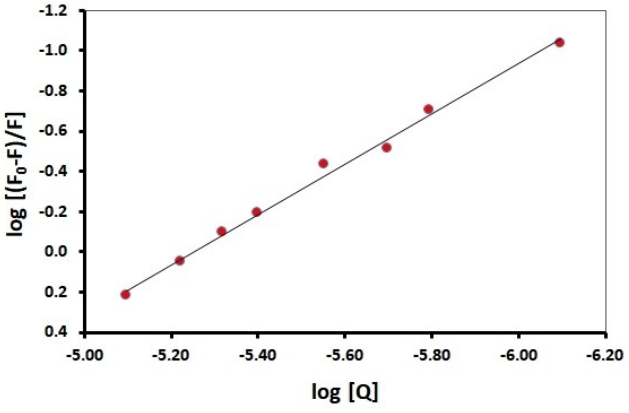

Figure 9. Plots of log $(F_0\text{-}F)/F$ versus log [Q] for complex **3**.

Table 4. The HSA binding constants and parameters (K_{SV}, k_q, K, n) for the ligands **1** and **2**, and complexes **3** and **4**.

Compd.	K_{SV}[a]	k_q[b]	R^2[c]	K[a]	n	R^2[c]
1	5.52×10^4	5.52×10^{12}	0.991	6.32×10^5	1.21	0.996
2	1.92×10^4	1.92×10^{12}	0.981	5.74×10^4	1.09	0.991
3	2.15×10^5	2.15×10^{13}	0.985	3.62×10^6	1.25	0.994
4	1.24×10^5	1.24×10^{13}	0.982	1.04×10^6	1.19	0.992

[a] M^{-1}. [b] M^{-1} s^{-1}. [c] R is the correlation coefficient.

binding force between complex and HSA, which implies that HSA can enable transfer complex towards potential bio-targets. As shown in Table 4, ligands have a lower binding affinity for albumin in relation to their complexes.

A simple method to investigate structural changes of HSA in the presence of the complex, as well as to determine the type of quenching is UV-Vis absorption spectroscopy. Quenching usually occurs either by the dynamic or static mechanism. Collisional (dynamic) quenching only affects the excited states of the fluorophores and, thus, no changes in the absorption spectra. In contrast, the ground state complex formation will frequently result in perturbation of the absorption spectrum of the fluorophore.[36] In the present study, the change in the UV-Vis absorption spectra of the HSA-complex system (Figure 10 and Figure S14 in the Supporting Information) was measured under simulated physiological conditions. HSA has a weak absorption peak at about 280 nm because of the cumulative absorption of three aromatic amino acid residues (Trp, Tyr, and Phe). The absorption intensity at 280 nm increased progressively (Figure 10 and Figure S14 in the Supporting Information) with the addition of complexes 3 and 4 and ligands 1 and 2, suggesting that the complex was formed between ligand or complex and HSA and that there exists a static interaction between HSA and the added compounds due to the formation of the ground state complex of the type of HSA compound.

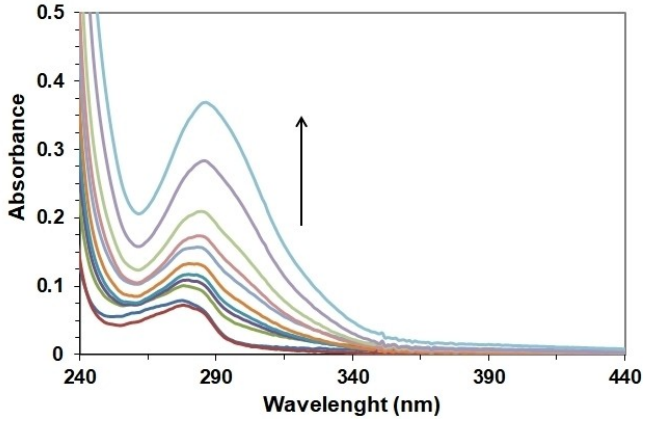

Figure 10. Absorption spectra of HSA (2.0 μM), with various amounts of the complex **3** (0-16 2.0 μM) at room temperature.

Table 5. Bond length X-Ray vs. DFT for complex **3**.[a] and bond length DFT of complex 4.[a]

Complex **3**				Complex **4**	
X-Ray		DFT		DFT	
Ru1-N1	2.059 (2)	Ru1-N5	2.059 (1)	Ru1-N5	2.058 (1)
Ru1-C18	2.150 (3)	Ru1-C12	2.152 (1)	Ru1-C12	2.157 (1)
Ru1-C20	2.159 (3)	Ru1-C15	2.164 (1)	Ru1-C15	2.167 (1)
Ru1-C19	2.176 (3)	Ru1-C11	2.211 (1)	Ru1-C10	2.183 (1)
Ru1-C21	2.190 (3)	Ru1-C7	2.181 (1)	Ru1-C7	2.179 (1)
Ru1-C17	2.195 (3)	Ru1-C10	2.183 (1)	Ru1-C18	2.186 (1)
Ru1-C16	2.211 (3)	Ru1-C18	2.190 (1)	Ru1-C11	2.208 (1)
Ru1-Cl1	2.409 (8)	Ru1-Cl2	2.439 (1)	Ru1-Cl2	2.439 (1)
Ru1-Cl2	2.428 (8)	Ru1-Cl3	2.464 (1)	Ru1-Cl3	2.464 (1)
S1-N2	1.655 (3)	S4-N8	1.655 (1)	S4-N8	1.656 (1)

[a] [Å].

2.5. Computational chemistry

2.5.1 Quantum mechanics

We have optimized geometries of each isothiazole ligand and corresponding ruthenium(II) complex. To search for global minima, we have chosen the M06 method[39] and def2-TZVP[40] basis set as implemented in Gaussian09.[41] Ligands and complexes were left for full optimizations without restrictions (symmetry, restrains or constrains). Structural features (bonds, angles, and torsions) of the structures optimized are in good agreement with the experimental ones (Table 5). DFT optimized structure of the X-ray non-resolved complex **4** is given in Figure 11, showing structural resemblance with structure **3**.

2.5.2. TD-DFT

Electronic spectra of the complexes exhibit wide absorption band that originates from d–d transitions and the intense bands coming from ligand to metal charge-transfer. The UV–Vis spectra of the complexes are similar and show d–d bands in the ranges 420–500 nm and 300–350 nm attributed to $^1A_1 \rightarrow {}^1A_2$, $^1A_1 \rightarrow {}^1B_1$, and $^1A_1 \rightarrow {}^1B_2$ transitions in pseudo-octahedral geometry of these complexes (Figure 12, Table S2 in the Supporting Information).

For these complexes, the nature of the transitions observed in the UV–Vis spectra have been studied by the time-dependent density functional (TD-DFT) method based on the optimized geometries, without any symmetry restrictions, in the singlet states. The IEFPCM solvent model was used in the Gaussian calculations with methanol as the solvent. The experimental spectrum of complex **3** with the calculated

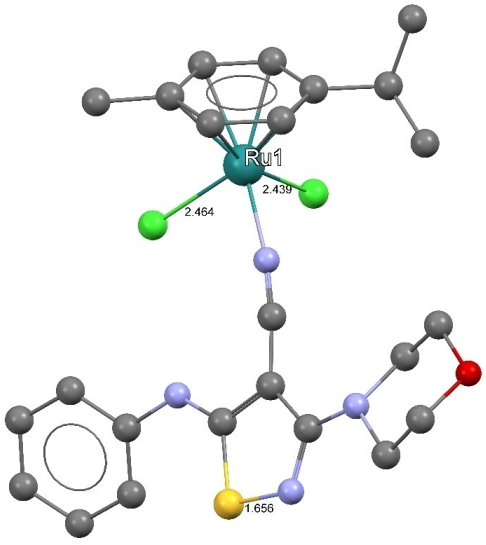

Figure 11. MERCURY[28] drawing of M06/def2-TZVP optimized structure of the complex **4**.

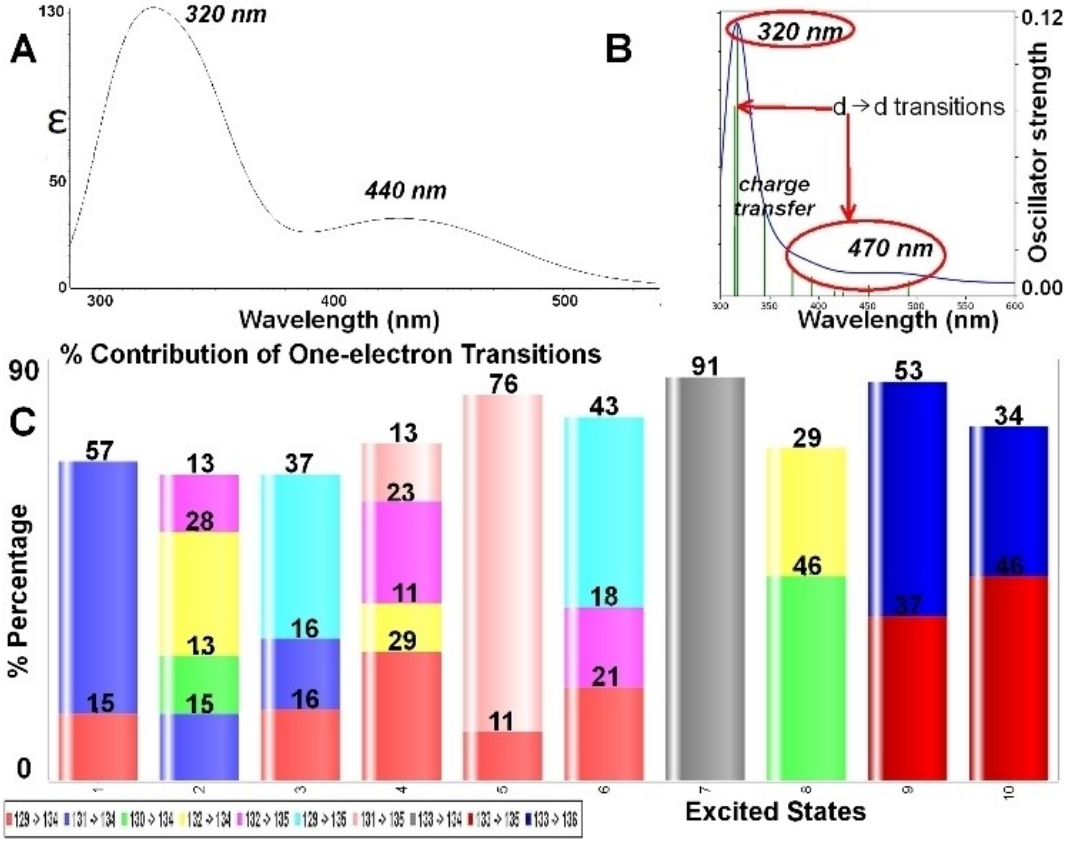

Figure 12. Experimental and TD-DFT UV spectra of the complex **3**: A) experimental UV-Vis spectra; B) calculated TD-DFT spectra; C) contribution of One-electron transitions.

transitions is presented in Figure 12 (Table S2 in the Supporting Information). The electronic transitions were calculated with use of M06/def2-TZVP method/bs. The assignments of the calculated transitions to the experimental bands are based on the criteria of their energies and oscillator strengths. Only the main components of the molecular orbitals are taken into consideration.

The experimental bands in the range 300–500 nm are assigned to the transitions between the frontier HOMO + n (see Figure 12) and LUMO molecular orbitals. As most of the highest occupied and lowest virtual molecular orbitals are composed of the d ruthenium orbitals the transitions are described by Ligand Field type (d→d). Only transitions No. 7, 9 and 10 involve mainly pure HOMO MO that, in addition, has a ligand character, and as a whole have metal-ligand charge transfer character.

2.5.3. Molecular docking

A number of different processes, including ligand substitution and formation of aqua complexes, appear to determine the fate of the metal complex in vivo. Like cisplatin, ruthenium(II)-arene complexes remain predominantly in their less reactive chloride form at high chloride concentrations (such as in the human bloodstream). At low chloride concentrations (e.g. inside a human cell) hydrolysis of complexes $Cl \leftrightarrow H_2O$ is expected,[42] activating them toward reactions with DNA.[43] For the same type of complexes, [Ru(η^6-*p*-cymene)(PTA)Cl_2] Scolaro et al. established that [Ru(η^6-*p*-cymene)(PTA)Cl(H_2O)]$^+$ hydrolytic product was the most abundant one.[42] Therefore, we decided that our modeling and simulation research is based on aqua species of ruthenium(II) complexes with isothiazoles **1** and **2**.

In this paper, we used AutoDock[44] and AutoDock Vina[45] software for the docking of ruthenium complexes on DNA molecule which structure is already determined by means of crystallography (PDB code 1AIO). For the purpose of docking run, we have chosen centers of minor and major grooves for the grid box and left ligands and ruthenium(II) complexes to dock on the rigid DNA. In our case, the ruthenium(II) complexes exerted much lower minor groove ΔG binding energies than that was the case with major groove only the results of the best hits of docking simulation are given in Table 6.

We may see that a kind of consistency between Vina and AutoDock results occurs but our validation study which was done on several DNA-Ru^{II} complexes (Figure S15 in the Supporting Information) indicates AutoDock as a method of choice. It is to be pointed out that predicted and experimental $\Delta G_{binding}$ values in case of *bis*-aqua complexes (ΔG was calculated using experimentally determined K_b, Table 3) are in

Table 6. Docking results of ligands and corresponding [Ru(η^6-*p*-cymene)X_2(L)] (X = H_2O) or [Ru(η^6-*p*-cymene)XY(L)] (X = H_2O and Y=Cl) complexes toward DNA.

Compound	AutoDock ΔG[a]	K_i[b]	Vina Affinity[a]	Exp. ΔG[a]
1	−3.79	1.67 [c]	−6.80	−6.14
2	−3.71	1.90 [c]	−6.90	−6.23
[Ru(η^6-*p*-cymene)(**1**)$(H_2O)_2$]$^{2+}$	**−6.82**	10.06	−8.00	**−6.71**
[Ru(η^6-*p*-cymene)Cl(**1**)(H_2O)]$^{+}$	−5.38	113.50	−7.00	/
[Ru(η^6-*p*-cymene)(**2**)$(H_2O)_2$]$^{2+}$	**−6.06**	36.41	−8.10	**−6.35**
[Ru(η^6-*p*-cymene)Cl(**2**)(H_2O)]$^{+}$	−5.02	210.26	−7.60	/

[a] kcal mol^{-1}. [b] μM. [c] mM.

very good agreement (Table 6). We have investigated the nature of docked interactions between DNA and the best hits of ligands and complexes as well (Figure 13).

Interactions of the investigated compounds with the DNA (Figure 14, Table S3 in the Supporting Information) were determined using Discovery Studio Visualizer.[46] All the investigated compounds were found to interact with the deoxythymidine 5 (DT5) from the A chain and with deoxycytidine 18 (DC18) in the B chain of the DNA. Carbonyl group in thymine of DT5 acts as a proton acceptor in a hydrogen bond with a hydrogen atom on nitrogen from phenylamino group in case of **1**, **3**, and **4**, but in the case of **2**, same carbonyl group interacts with an equatorial hydrogen atom on carbon that is adjacent to oxygen of the morpholine group. That allows phenylamino group in **2** to act as a hydrogen donor in a hydrogen bond with phosphate of deoxyadenosine 17 (DA17). Cytosine amino group of DC18 interacts as a hydrogen donor with π electrons of phenyl group that is connected to isothiazole via nitrogen in the case of **3** and **4**. In the case of **2** same amino group acts as a hydrogen donor in interaction with the carbonitrile group, while it does not interact in any way with **1**. Ligand **1** is instead positioned to interacts with π electrons of cytosine in DC18 via sulfur. That position allows **1**'s carbonitrile group to act as a hydrogen acceptor in a hydrogen bond with guanine from deoxyguanosine 6 (DG6). In both **3** and **4**, one of the coordinated water molecules interacts with phosphate of DT5 and phosphate of deoxycytidine 4 (DC4) forming two hydrogen bonds.

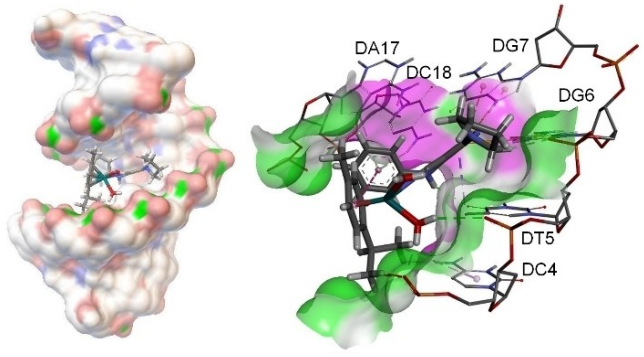

Figure 13. The best hit (AutoDock) of hydrolyzed complex **3** docked on DNA (left) and basic DNA-Complex **3** interactions (right).

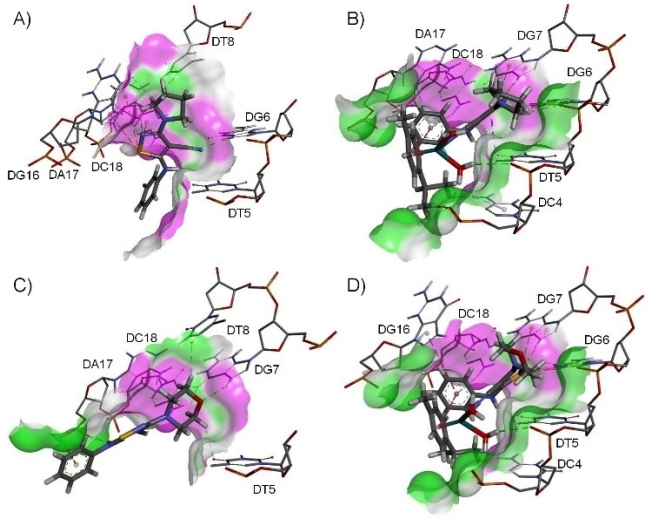

Figure 14. DNA–L interactions by ligand's binding within major groove.

2.6. Biological tests

2.6.1 In vitro cytotoxic activity of ligands and complexes

The cytotoxic activity of ligands and complexes was examined on HeLa and HCT116 tumor cell lines and non-tumor MRC-5 cells line using MTT assay (Table 7). Because of the possible coordination of S atoms from DMSO with the ruthenium,[47] before biological experiments we tested the chemical stability of the complexes in DMSO using ^{1}H NMR spectroscopy. Compared with the ^{1}H NMR spectra in $CDCl_3$, the proton chemical shifts of ruthenium complexes in DMSO-d_6 are slightly

Table 7. IC_{50} (μM) values determined by MTT assay for ligands **1** and **2** and complexes **3** and **4** after 24 h and 48 h treatment of HeLa, HCT116 and MRC-5 cells and SI values.[a]

IC_{50}	24 h	SI [b]	48 h	SI [b]
	HeLa			
1	135.25 ± 44.7	1.67	83.59 ± 18.18	2.71
2	77.43 ± 14.11	3.24	100.74 ± 14.95	2.49
3	194.48 ± 45.39	2.35	103.20 ± 14.87	4.13
4	200.5 ± 46.36	0.76	98.6 ± 3.4	1.30
***cis*Pt**	14.506 ± 4.068	/	14.391 ± 2.750	/
	HCT116			
1	2431.94 ± 342.8	0.09	106.7 ± 19.6	1.93
2	175.39 ± 10.20	1.43	60.98 ± 10.11	1.87
3	59.12 ± 5.2	7.72	33.96 ± 12.1	12.55
4	95.91 ± 4.5	1.58	54.45 ± 9.3	2.37
***cis*Pt**	39.372 ± 0.591	/	20.480 ± 6.984	/
	MRC-5			
1	226.45 ± 42.03	/	206.45 ± 52.4	/
2	250.64 ± 16.4	/	113.90 ± 20.08	/
3	456.68 ± 101.83	/	426.15 ± 64.18	/
4	151.70 ± 37.33	/	129.11 ± 11.05	/
***cis*Pt**	49.37 ± 10.064	/	16.270 ± 6.265	/

[a] IC_{50} values (μM) expressed as the X ± SD. [b] SI-selectivity index.

moved due to the different polarity of solvent (Figure S16 in the Supporting Information). These data indicated that the structure of examined Ru^{II} complexes remains stable in DMSO solution for at least 48 h. MTT test results showed that all tested compounds decreased cell viability in all three cell lines in a dose-dependent manner (Figure S17 in the Supporting Information). Obtained data were used to calculate IC_{50} values for each compound after 24 and 48 h incubation. As shown in Table 7, both ligands and complexes showed weak cytotoxic activity against healthy MRC-5 cells and to some extent stronger cytotoxic activity against HeLa cells, but on both cell lines IC_{50} values for tested compounds were high. Many isothiazole derivatives were tested for their cytotoxic activity in different tumor cell lines. They displayed diverse effects, from low to high cytotoxicity and various selectivity, depending on its structure and tested cell line.[20,21] Isothiazole ligands investigated in this study did not show notable cytotoxicity against both tumor cell lines. Although ligands **1** and **2** showed good selectivity for HeLa cells, their IC_{50} values in this cell line were high. On the other hand, HCT116 cells, sparingly sensitive to ligands, were susceptible to complexes **3** and **4**, as indicated by moderate IC_{50} values (33.96 μM and 54.45 μM, respectively, after 48 h incubation). However, the action of complex **4** was selective (SI after 48 h was 2.37), while complex **3** was highly selective for HCT116 cells (SI = 12.55), in contrast to low selectivity of *cis*Pt for the same cell line. It is obvious that the Ru^{II} complexes have more biological activity than the free ligands, which can be explained by the coordination effect. Platinum-based drugs, although efficacious in the therapy of many types of tumors show a number of side-effects. Thus, metal complexes that have strong and selective cytotoxic activity against tumor cells are the subject of many investigations. Based on these two criteria, we choose complexes **3** and **4** for further examination on the HCT116 cell line.

2.6.2. Complexes 3 and 4 induce apoptosis in HCT116 cells

Flow cytometric analysis of Annexin V-FITC/7-AAD stained cells showed that both complex **3** and **4** induce apoptosis in HCT116 cells (Figure 15). After 48 h treatment, the majority of cells were early apoptotic (22.98 % and 24.82 %, respectively),

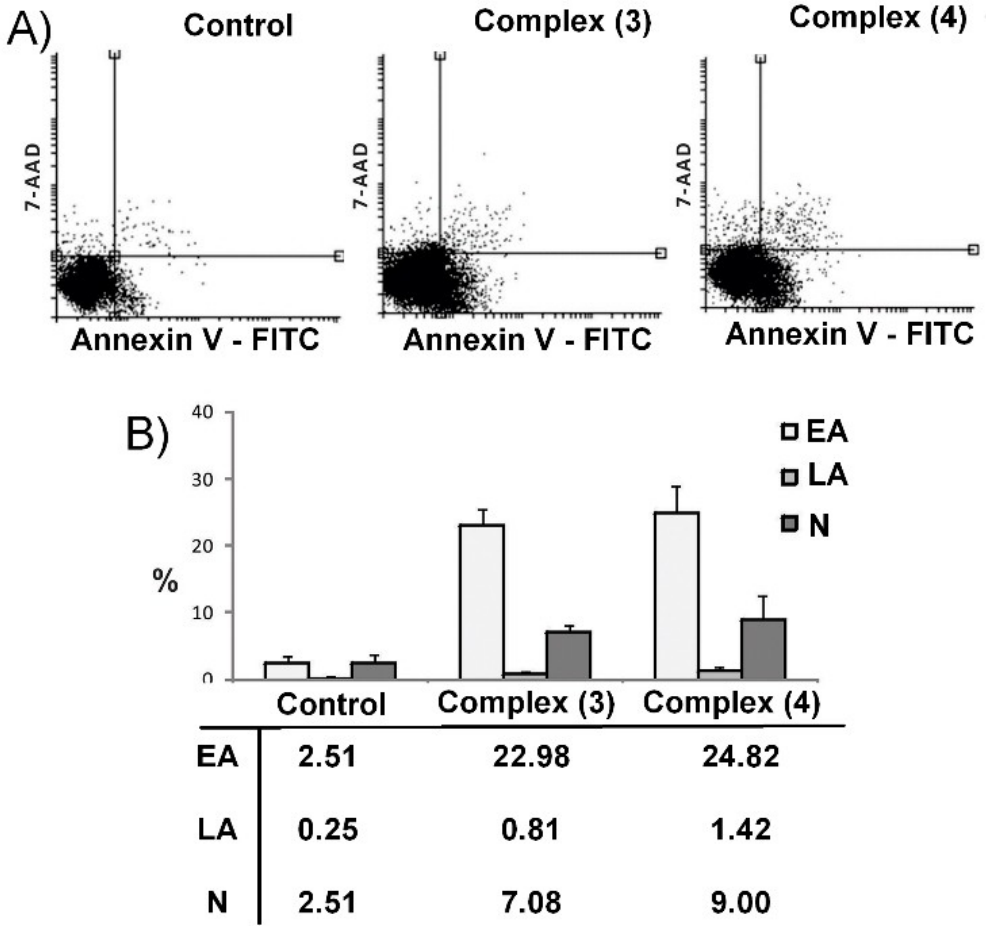

Figure 15. Flow cytometric analysis of Annexin V-FITC/7-AAD staining. (**A**) Dot plots presenting the percentage of viable (lower left quadrant), early apoptotic (lower right quadrant), late apoptotic (upper right quadrant) and necrotic cells (upper left quadrant). (**B**) Graph showing the percent of early apoptotic (EA), late apoptotic (LA) and necrotic cells (N) in untreated (control) and complex **3** and complex **4**-treated HCT116 cells. Results are presented as an average of three independent experiments.

while only a small percent of cells was late apoptotic or necrotic.

Necrosis is characterized as passive, accidental cell death that is accompanied by cell lysis and release of cellular content into extracellular surroundings, which consequently induce inflammation of adjacent tissue. On the other hand, apoptosis is an orderly type of cell death. Cell membrane remains intact, there is no induction of inflammation so that cells dying by apoptosis are not a threat for neighboring cells. For that reason, the induction of apoptosis is the desirable mechanism of action for cancer therapeutics.

2.6.3. Complexes 3 and 4 arrest cell cycle in S-phase

Exploring the mechanisms of action of complexes **3** and **4** we analyzed their effect on cell cycle progression (Figure 16). Our results showed that both tested complexes arrested HCT116 cells in S-phase of the cell cycle (control: 12.25 %; complex **3**: 62.05 %; complex **4**: 49.77 %).

Consequently, percent of cells in other phases of the cell cycle, especially in the G2/M phase, decreased. These data indicate a failure of proper chromosome replication, presumably because of DNA damage. Importantly, the increased number of polyploid (> 4 N) cells was observed in cells treated with complex **4**, indicating unsuccessful chromosome segregation, defined as mitotic catastrophe.[48] It is well known that the primary target of platinum-based drugs is DNA. These agents cause crosslinking of DNA that results in arresting cell cycle and activating repair mechanisms. If the DNA damage cannot be repaired, cells undergo apoptosis. In addition, Puig et al. showed that cisplatin may stop the mitotic activity of tumor cells, but without inhibition of DNA replication, engendering the appearance of giant polyploid cells.[49] Mitotic catastrophe restrains cell proliferation, leading to senescence, or affects survival, leading to apoptotic cell death. Cells undergoing mitotic catastrophe were detected by fluorescent microscopy after treatment of HCT116 cells with complex **4** as giant multinucleated cells (Figure 17).

It seems that mechanism of action of ruthenium(II) complexes shows similarity with platinum drugs, at least both arrest cell cycle in S-phase.

2.6.4. Complexes 3 and 4 induce autophagy in HCT116 cells

Autophagy is a natural mechanism for removing unnecessary or damaged cytoplasmic contents. As an adaptive response to stress, it promotes survival, but excessive autophagy can trigger cell death. Autophagy is characterized by the formation of autophagosomes which contain cellular components destined for degradation. These vesicles articulate with lysosomes to

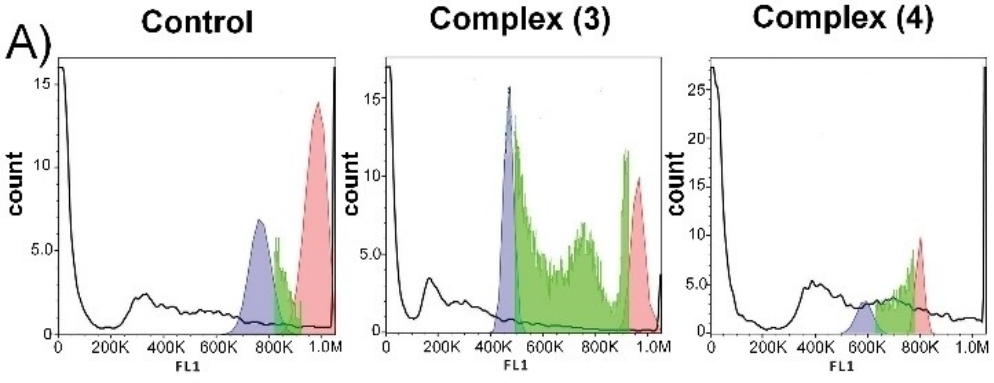

	Control	Complex (3)	Complex (4)
G0/G1	31.08	20.20	20.24
S	12.5	62.05	49.77
G2/M	56.67	17.75	29.98

Figure 16. Cell cycle analysis. (**A**) Histograms and (**B**) graph presenting cell cycle distribution in untreated HCT116 cells (control) and cells treated with complex **3** and complex **4**. Results are presented as an average of three independent experiments.

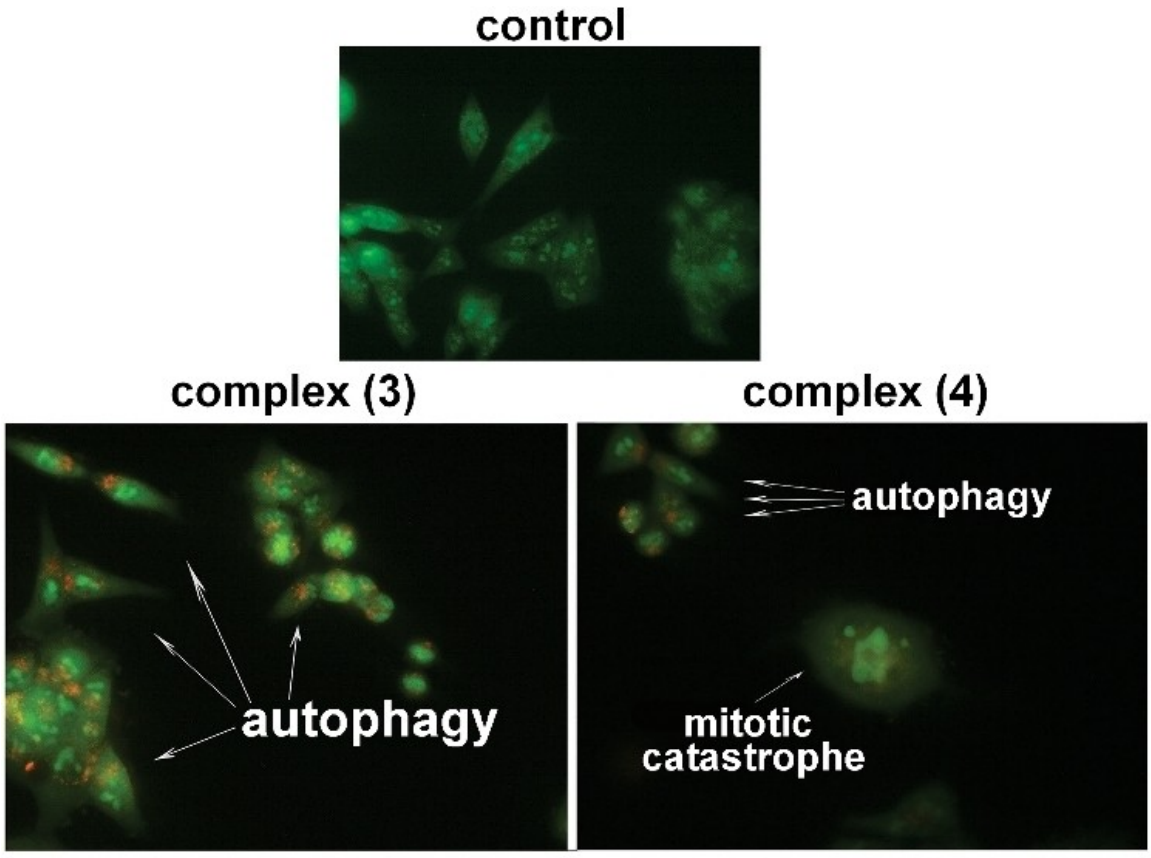

Figure 17. Representative images of AO stained HCT116 cells: untreated, treated with complex **3** and complex **4**.

form autophagolysosomes where hydrolases degradate autophagic content. Autophagy can be detected by microscopy using cell-permeable fluorescent dye acridine orange (AO). At neutral pH, in cytoplasm and nucleus, AO emits green fluorescence, but within acidic vesicles (AVOs) it emits bright red fluorescence. In order to detect the induction of autophagy, HCT116 cells were treated with tested complexes and stained with AO. Fluorescent microscopy showed an extensive amount of red AVOs in both complex **3** and complex **4**-treated cells, in contrast to untreated control with very few AVO-positive cells (Figure 16). This result indicates that the induction of autophagy is involved in mechanisms of action of both tested complexes.

3. Conclusion

In summary, two new neutral complexes were prepared from [Ru(η6-p-cymene)Cl2]2 and 3,5-diaminoisothiazole derivatives ligands: [Ru(η6-p-cymene)Cl2(1)] (3) and [Ru(η6-p-cymene Cl2 (2)] (4), where 1 = 5-(phenylamino)-3-pyrrolidin-1-ylisothiazole-4-carbonitrile; 2 = 3-morpholin-4-yl-5-(phenylamino)isothiazole-4-carbonitrile. Both complexes were characterized by spectroscopic (IR, UV-Vis, and NMR), but the crystal structure was confirmed only for complex 3. Besides, the structures of two early synthesized ligands 1 and 2 were confirmed. The DNA interaction and protein binding properties of the new complexes were evaluated by absorption and fluorescence spectroscopies. The present study of interaction with CT-DNA shows that ruthenium(II) complexes bind well intercalatively to CT-DNA. Too, all the ligands and the complexes show a good binding affinity to HSA protein giving relatively high binding constants. The complex 3 exhibits the highest K values among the compounds tested. Docking experiments toward DNA dodecamer have been done indicating an excellent accordance with experimental ΔG values.

The isothiazole ligands **1** and **2** did not show significant cytotoxicity to both tumor cell lines versus the corresponding complexes which can be explained by the coordination effect. Complex **3** is highly selective for HCT116 cells relative to complex **4**. Flow cytometric analysis of Annexin V-FITC/7-AAD stained cells showed that both complexes induce apoptosis in HCT116 cells with a cell cycle arrest in the S-phase. It seems that mechanism of action of ruthenium(II) complexes shows similarity with platinum drugs, at least both arrest cell cycle in S-phase. Mitotic catastrophe restrains cell proliferation, leading to senescence, or affects survival, leading to apoptotic cell death. Cells undergoing mitotic catastrophe were detected by fluorescent microscopy after treatment of HCT116 cells with complex 4 as giant multinucleated cells. Also, the induction of autophagy is involved in mechanisms of action of both tested complexes.

Deposition Numbers CCDC_1985935 (for **1**), CCDC_1985936 (for **2**) and CCDC_1985937 (for **3**) contains the supplementary crystallographic data for this paper. These data are provided free of charge by the joint Cambridge Crystallographic Data Centre www.ccdc.cam.ac.uk/structures.

Supporting Information Summary

The general experimental section including detailed synthetic procedure, analytical data, ^{1}HNMR, ^{13}CNMR, FT-IR and UV-Vis spectra, computational chemistry, as well as biological experimental procedures are provided in the Supporting Information. Also, crystal data and experimental details of the structure's determination for ligands 1 and 2, and complex 3 are included.

Acknowledgements

This work was supported by the Serbian Ministry of Education, Science and Technological Development (Agreement No. 451-03-68/2020-14/200122).

Conflict of Interest

The authors declare no conflict of interest.

Keywords: Antitumor activity · Isothiazole · Molecular docking · Ruthenium · X-ray diffraction

[1] a) B. Rosenberg, L. Van Camp, T. Krigas, *Nature* **1965**, *205*, 698–699; b) B. Rosenberg, L. Van Camp, J. E. Trosko, V. H. Mansour, *Nature* **1969**, *222*, 385–386.
[2] A. H. Calvert, S. J. Harland, D. R. Newell, Z. H. Siddik, A. C. Jones, T. J. McElwain, S. Raju, E. Wiltshaw, I. E. Smith, J. M. Baker, M. J. Peckham, K. R. Harrap, *Cancer Chemother. Pharmacol.* **1982**, *9*, 140–147.
[3] J. M. Extra, M. Espie, F. Calvo, C. Ferme, L. Mignot, M. Marty, *Cancer Chemother. Pharmacol.* **1990**, *25*, 299–303.
[4] J. Q. Wang, P. Y. Zhang, L. N. Ji, H. Chao, *J. Inorg. Chem.* **2015**, *146*, 89–96.
[5] a) Y. Yang, L. Guo, Z. Tian, X. Liu, Y. Gong, H. Zheng, X. Ge, Z. Liu, *Chem. Asian J.* **2018**, *13*, 2923–2933; b) A. Sarkar, S. Acharya, K. Khushvant, K. Purkait, A. Mukherjee, *Dalton Trans.* **2019**, *48*, 7187–7197; c) L. Zeng, P. Gupta, Y. Cheng, E. Wang, L. Ji, H. Chao, Z.-S. Chen, *Chem. Soc. Rev.* **2017**, *46*, 5771–5804.
[6] a) Y.-H. Dou, S.-D. Xu, Y. Chen, X.-H. Wu, *Phosphorus Sulfur* **2017**, *192*, 1219–1223; b) C. Scolaro, A. Bergamo, L. Brescacin, R. Delfino, M. Cocchietto, G. Laurenczy, T. J. Geldbach, G. Sava, P. J. Dyson, *J. Med. Chem.* **2005**, *48*, 4161–4171.
[7] a) L. Biancalana, G. Pampaloni, S. Zacchini, F. Marchetti, *J. Organomet. Chem.* **2017**, *848*, 214–221; b) S. M. Meier-Menches, C. Gerner, W. Berger, C. G. Hartinger, B. K. Keppler, *Chem. Soc. Rev.* **2018**, *47*, 909–928; c) F. Marchetti, R. Pettinari, C. Di Nicola, C. Pettinari, J. Palmucci, R. Scopelliti, T. Riedel, B. Therrien, A. Galindo, P. J. Dyson, *Dalton Trans.* **2018**, *47*, 868–878.
[8] a) C. S. Allardyce, P. J. Dyson, *Dalton Trans.* **2016**, *45*, 3201–3320; b) B. S. Murray, M. V. Babak, C. G. Hartinger, P. J. Dyson, *Coord. Chem. Rev.* **2016**, *306*, 86–114; c) A. A. Nazarov, C. G. Hartinger, P. J. Dyson, *J. Organomet. Chem.* **2014**, *751*, 251–260.
[9] a) R. L. Siegel, K. D. Miller, A. Jemal, *Ca-Cancer J. Clin.* **2018**, *68*, 7–30; b) A. Bergamo, G. Sava, *Dalton Trans.* **2011**, *40*, 7817–7823.
[10] a) M. Djukić, M. S. Jeremić, R. Jelić, O. Klisurić, V. Kojić, D. Jakimov, P. Djurdjević, Z. D. Matović, *Inorg. Chim. Acta* **2018**, *483*, 359–370; b) S. Parveen, F. Arjmand, S. Tabassum, *Eur. J. Med. Chem.* **2019**, *175*, 269–286.
[11] a) H. Chen, J. A. Parkinson, S. Parsons, R. A. Coxall, R. O. Gould, P. J. Sadler, *J. Am. Chem. Soc.* **2002**, *124*, 3064–3082; b) H. Chen, J. A. Parkinson, R. E. Morris, P. J. Sadler, *J. Am. Chem. Soc.* **2003**, *125*, 173–186.
[12] Z. Adhireksan, G. E. Davey, P. Campomanes, M. Groessl, C. M. Clavel, H. Yu, A. A. Nazarov, C. H. F. Yeo, W. H. Ang, P. Dröge, U. Rothlisberger, P. J. Dyson, C. A. Davey, *Nat. Commun.* **2014**, *5*, 3462.
[13] A. De Oliveira Silva, J. McQuade, M. Szostak, *Adv. Synth. Catal.* **2019**, *361*, 3050–3067.
[14] A. Adams, R. Slask, Chem. Ind. (London) **1956**, *42*, 1232.
[15] a) F. Clerici, E. Erba, M. L. Gelmi, M. Valle, *Tetrahedron* **1997**, *53*, 15859–15866; b) T. V. Omelian, A. V. Dobrydnev, E. N. Ostapchuk, Y. M. Volovenko , *ChemistrySelect* **2019**, *4*, 4933–4937; c) Q.-F. Wu, B. Zhao, Z.-J. Fan, J.-B. Zhao, X.-F. Guo, D.-Y. Yang, N.-L. Zhang, B. Yu, T. Kalinina, T. Glukhareva, *RSC Adv.* **2018**, *8*, 39593–39601; d) E. A. Dikusar, S. K. Petkevich, N. A. Zhukovskaya, T. D. Zvereva, P. V. Kurman, *Russ. J. Org. Chem.* **2019**, *55*, 462–468.
[16] a) M. T. Cocco, V. Onnis, *Synthesis* **1993**, 199–201; b) M. T. Cocco, C. Congiu, A. Maccioni, V. Onnis, M. L. Schivo, A. De Logu, *Il Farmaco* **1994**, *49*, 137–140.
[17] A. Garozzo, M. R. Pinizzotto, F. Guerrera, G. Tempera, A. Castro, E. Geremia, *Arch. Virol.* **1994**, *135*, 1–11.
[18] V. Mishra, T. S. Chundawat, *Turk. J. Chem.* **2019**, *43*, 713–729.
[19] K. I. Reddy, K. Srihari, J. Renuka, K. S. Sree, A. Chuppala, V. U. Jeankumar, J. P. Sridevi, K. S. Babu, P. Yogeeswari, D. Sriram, *Bioorg. Med. Chem.* **2014**, *22*, 6552–6563.
[20] I. Jęśkowiak, M. Mączyński, J. Trynda, J. Wietrzyk, S. Ryng, *Bioorg. Chem.* **2019**, *91*, 103082–103090.
[21] S. Rao Ambati, S. Gudala, A. Sharma, S. Penta, V. Loka Reddy, Y. Bomma, V. Rao, Janapala, S. Pola, *J. Heterocycl. Chem.* **2017**, *54*, 2333–2341.
[22] C. V. N. S. Varaprasad, D. Barawkar, H. El Abdellaoui, S. Chakravarty, M. Allan, H. Chen, W. Zhang, J. Z. Wu, R. Tam, R. Hamatake, S. Lang, Z. Hong, *Bioorg. Med. Chem. Lett.* **2006**, *16*, 3975–3980.
[23] B. Lippa, J. Morris, M. Corbett, T. A. Kwan, M. C. Noe, S. L. Snow, T. G. Gant, M. Mangiaracina, H. A. Coffey, B. Foster, E. A. Knauth, M. D. Wessel, *Bioorg. Med. Chem. Lett.* **2006**, *16*, 3444–3448.
[24] a) V. V. Semenov, B. V. Lichitsky, A. N. Komogortsev, A. A. Dudinov, M. M. Krayushkin, L. D. Konyushkin, O. P. Atamanenko, I. B. Karmanova, Y. A. Strelenko, B. Shor, M. N. Semenova, A. S. Kiselyov, *Eur. J. Med. Chem.* **2017**, *125*, 573–585; b) A. S. Kiselyov, M. N. Semenova, N. B. Chernyshova, A. Leitao, A. V. Samet, K. A. Kislyi, M. M. Raihstat, T. Oprea, H. Lemcke, M. Lantow, D. G. Weiss, N. N. Ikizalp, S. A. Kuznetsov, V. V. Semenov, *Eur. J. Med. Chem.* **2010**, *45*, 1683–1697.
[25] V. Berdini, T. R. Early, M. A. O'Brien, A. J. Woodhead, P. G. Wyatt, *PCT Int. Appl.* **2006**, WO2006008545.
[26] A. S. Kiselyov, M. Semenova, V. V. Semenov, *Bioorg. Med. Chem. Lett.* **2009**, *19*, 1195–1198.
[27] a) K. N. Kumar, G. Venkatachalam, R. Ramesh, Y. Liu, *Polyhedron* **2008**, *27*, 157–166; b) A. Juris, L. Prodi, A. Harriman, R. Ziessel, M. Hissler, A. El-ghayoury, F. Wu, E. C. Riesgo, R. P. Thummel, *Inorg. Chem.* **2000**, *39*, 3590–3598; c) J. V. Ortega, K. Khin, W. E. van der Veer, J. Ziller, B. Hong, *Inorg. Chem.* **2000**, *39*, 6038–6050; d) R. N. Prabhu, D. Pandiarajan, R. Ramesh, *J. Organomet. Chem.* **2009**, *694*, 4170–4177; e) J. M. Gichumbi, H. B. Friedrich, B. Omondi, *J. Organomet. Chem.* **2016**, *808*, 87–96.
[28] I. J. Bruno, J. C. Cole, P. R. Edgington, M. K. Kessler, C. F. Macrae, P. McCabe, J. Pearson, R. Taylor, *Acta Crystallogr.* **2002**, *B58*, 389–397.
[29] C. X. Zhang, S. J. Lippard, *Curr. Opin. Chem. Biol.* **2003**, *7*, 481–489.
[30] E. Ramachandrana, D. S. Raja, N. S. P. Bhuvanesh, K. Natarajan, *Dalton Trans.* **2012**, *41*, 13308–13323.
[31] Z. C. Liu, B. D. Wang, B. Li, Q. Wang, Z. Y. Yang, T. R. Li, Y. Li, *Eur. J. Med. Chem.* **2010**, *45*, 5353–5361.
[32] A. Ambroise, B. G. Maiya, *Inorg. Chem.* **2000**, *39*, 4264–4272.
[33] S. A. Tysoe, R. J. Morgan, A. D. Baker, T. C. Strekas, *J. Phys. Chem.* **1993**, *97*, 1707–1711.
[34] A. Wolf, G. H. Shimer, T. Meehan, *Biochemistry* **1987**, *26*, 6392–6396.
[35] W. D. Wilson, L. Ratmeyer, M. Zhao, L. Strekowski, D. Boykin, *Biochemistry* **1993**, *32*, 4098–4104.
[36] J. R. Lakowicz, *Principles of Fluorescence Spectroscopy*, Springer, New York, USA, 3rd edn, **2006**.
[37] J. R. Lakowicz, G. Weber, *Biochemistry* **1973**, *12*, 4161–4170.

[38] J. D. Berić, S. D. Stojanović, E. M. Mrkalić, Z. D. Matović, D. R. Milovanović, M. M. Sovrlić, R. M. Jelić, *Monatsh. Chem.-Chemical Monthly* **2018**, *149*, 2359–2368.
[39] Y. Zhao, D. G. Truhlar, *Theor. Chem. Acc.* **2008**, *120*, 215–241.
[40] F. Weigend, R. Ahlrichs, *Phys. Chem. Chem. Phys.* **2005**, 7, 3297–3305.
[41] M. J. Frisch, G. W. Trucks, H. B. Schlegel, G. E. Scuseria, M. A. Robb, J. R. Cheeseman, G. Scalmani, V. Barone, B. Mennucci, G. A. Petersson, H. Nakatsuji, M. Caricato, X. Li, H. P. Hratchian, A. F. Izmaylov, J. Bloino, G. Zheng, J. L. Sonnenberg, M. Hada, M. Ehara, K. Toyota, R. Fukuda, J. Hasegawa, M. Ishida, T. Nakajima, Y. Honda, O. Kitao, H. Nakai, T. Vreven, J. A. Montgomery Jr., J. E. Peralta, F. Ogliaro, M. Bearmark, J. J. Heyd, E. Brothers, K. N. Kudin, V. N. Staroverov, R. Kobayashi, J. Normand, K. Raghavachari, A. Rendell, J. C. Burant, S. S. Iyengar, J. Tomasi, M. Cossi, N. Rega, J. M. Millam, M. Klene, J. E. Knox, J. B. Cross, V. Bakken, C. Adamo, J. Jaramillo, R. Gomperts, R. E. Stratmann, O. Yazyev, A. J. Austin, R. Cammi, C. Pomelli, J. W. Ochterski, R. L. Martin, K. Morokuma, V. G. Zakrzewski, G. A. Voth, P. Salvador, J. J. Dannenberg, S. Dapprich, A. D. Daniels, O. Farkas, J. B. Foresman, J. V. Ortiz, J. Cioslowski, D. J. Fox, Gaussian 09, Revision D.01 ed., Gaussian, Inc., Wallingford CT, USA, **2013.**
[42] C. Scolaro, C. G. Hartinger, C. S. Allardyce, B. K. Keppler, P. J. Dyson, *J. Inorg. Biochem.* **2008**, *102*, 1743–1748.
[43] a) F. Wang, J. Bella, J. A. Parkinson, P. J. Sadler, *J. Biol. Inorg. Chem.* **2005**, *10*, 147–155; b) F. Wang, J. Xu, A. Habtemariam, J. Bella, P. J. Sadler, *J. Am. Chem. Soc.* **2005**, *127*, 17734–17743.
[44] G. M. Morris, R. Huey, W. Lindstrom, M. F. Sanner, R. K. Belew, D. S. Goodsell, A. J. Olson, *J. Comput. Chem.* **2009**, *30*, 2785–2791.
[45] O. Trott, A. J. Olson, *J. Comput. Chem.* **2010**, *31*, 455–461.
[46] Dassault Systèmes BIOVIA, Discovery Studio, v.17.2.0, **2016**.
[47] M. Patra, T. Joshi, V. Pierroz, K. Ingram, M. Kaiser, S. Ferrari, B. Springler, J. Keiser, G. Gasser, *Chem. Eur. J.* **2013**, *19*, 14768–14772.
[48] L. Galluzzi, I. Vitale, S. A. Aaronson, J. M. Abrams, D. Adam, P. Agostinis et al., *Cell Death Differ.* **2018**, *3*, 486–541.
[49] P. E. Puig, M. N. Guilly, A. Bouchot, N. Droin, D. Cathelin, F. Bouyer, L. Favier, F. Ghiringhelli, G. Kroemer, E. Solary, F. Martin, B. Chauffert, *Cell Biol. Int.* **2008**, *32*, 1031–43.

Submitted: July 7, 2020
Accepted: September 16, 2020